Published as: *Science*. 2012 January 27; 335(6067): 436–441.

Crystal structure of the human K2P TRAAK, a lipid- and mechano-sensitive K^+ ion channel

Stephen G. Brohawn[1], **Josefina del Mármol**[1], and **Roderick MacKinnon**[1]

[1]Laboratory of Molecular Neurobiology and Biophysics, The Rockefeller University, Howard Hughes Medical Institute, 1230 York Avenue, New York, New York 10065, USA

Abstract

TRAAK channels, members of the two pore domain K^+ channel family, are expressed almost exclusively in the nervous system and control the resting membrane potential. Their gating is sensitive to polyunsaturated fatty acids, mechanical deformation of the membrane, and temperature changes. Physiologically these channels appear to control the noxious input threshold for temperature and pressure sensitivity in dorsal root ganglia neurons. We present the crystal structure of human TRAAK at 3.8 Å resolution. The channel comprises two protomers, each containing two distinct pore domains, which create a two-fold symmetric K^+ channel. The extracellular surface features a 35 Å tall helical cap that creates a bifurcated pore entryway and accounts for the insensitivity of two pore K^+ channels to inhibitory toxins. Two diagonally opposed gate-forming inner helices form membrane interacting structures that may underlie this channel's sensitivity to chemical and mechanical properties of the cell membrane.

Cellular electrical signaling relies upon a resting potential difference that originates in the membrane's permeability to K^+ (1). Termed "potassium leakage" by Hodgkin and Huxley (2), cellular leak currents are approximated by the behavior of constitutively open K^+-selective pores, but deviate in detail, suggesting more complex underlying channel behavior. Leak K^+ currents are now recognized to be due to the activity of "two pore domain" K^+ ion channels (K2P channels) (3). Discovered as the final member of the K^+ channel family (4–6), their molecular and biophysical characterization has lagged behind that of other K^+ channels. Perhaps the prospect of studying simple "leakage" has somewhat delayed progress.

The view of K2P channels as passive K^+ leaks has recently changed. K2P channels control the resting potential in many cells and their regulation can directly tune cellular excitability. K2P channels have among the most varied sets of ion channel modulators including mechanical force, temperature, lipid interaction, voltage, pH, posttranslational modification, and accessory protein interaction (3, 7, 8). Pharmacologically, K2P channels are targets of antidepressants, inhalational anesthetics, neuroprotective agents, and respiratory stimulants (9–12). Their deregulation underlies human pathophysiologies including Birk-Barel syndrome and familial migraine with aura (13, 14).

K2P channels form one of five clades within the K^+ channel superfamily (fig. S1A,B). While sequence diverse (figs. S1C, S2), two shared characteristics define K2P channels. First, K2P channels contain two concatenated pore domains on a single protein chain protomer (fig. S1A). Each of the pore domains contain an outer and inner membrane-spanning helix flanking a membrane-reentrant segment that forms a pore helix and K^+ selectivity filter. K^+ channels of known structure have one pore domain per protomer and form four-fold symmetric tetramers. Second, K2P channels contain a segment of ~60 amino acids on the extracellular side of first pore domain. This segment has often been referred to as a "loop" and its role in channel function has been unknown.

The best-studied subfamily of K2P channels includes TRAAK (TWIK-related arachidonic acid-stimulated K^+ channel), TREK-1, and TREK-2 (fig. S3) (15–17). Unlike other K2P channels, they are mechanosensitive and modulated by polyunsaturated fatty acids and temperature (18–21). Physiologically, TRAAK and TREK-1 appear to regulate the noxious input threshold for temperature and pressure sensitivity in mouse dorsal root ganglia (22). These channels are highly sensitive to the structure and chemical composition of the lipid bilayer, but a mechanistic rationale for these biophysical properties has not been possible in the absence of structural information.

Crystal structure of TRAAK

Human TRAAK was recombinantly expressed and purified from *P. pastoris.* To obtain diffracting crystals, two consensus N-linked glycosylation sites were mutated (N104Q, N108Q) and the predicted intrinsically unstructured C-terminal region was truncated (to Q300). Four complementary approaches were taken to assess the functional integrity of this modified construct. First, macroscopic currents were examined in cells expressing TRAAK (Fig. 1A). Channels displayed approximate time- and voltage- independence of activation. Current-voltage relationships do not indicate strong rectification. Expressed channels were K^+ selective as demonstrated by the change in reversal potential as a function of external [K^+] (Fig. 1A, inset). Second, channel activation by arachidonic acid and mechanical force was examined. TRAAK channels are robustly activated above basal levels after perfusion of arachidonic acid (Fig. 1B). The extent of activation above basal levels by arachidonic acid is comparable to that measured from full-length TRAAK channels (Fig. 1C). Application of positive pressure through the pipette to outside-out patches also activated TRAAK channels (fig. S4). A more quantitative assessment of the gating response to mechanical perturbation will require in the future simultaneous measurements of pressure and membrane curvature to ascertain tension as the independent variable (23). Third, purified TRAAK was reconstituted into lipid vesicles and examined in a K^+ flux assay. A decrease in fluorescence indicative of K^+ flux was observed from TRAAK reconstituted, but not empty, vesicles loaded with high [K^+] into buffer without K^+ (Fig. 1D). Fourth, recordings were made with planar lipid bilayers into which purified TRAAK channels were reconstituted (Fig. 1E). The bilayer recordings show voltage-independent channels exhibiting exquisite selectivity for K^+ over Na^+ (Fig. 1F). Taken together these data show that the channel we have expressed, purified and crystallized exhibits the fundamental biophysical properties of previously described TRAAK channels (24).

Crystals of TRAAK grown in 150 mM KCl diffracted to 3.8 Å. Initial attempts at molecular replacement using known K^+ channel structures were unsuccessful. The structure was thus solved with phases determined from a multiple wavelength isomorphous replacement with anomalous scattering experiment using a crystal grown in the presence of $TlNO_3$ substituted for KCl. Additional register information was obtained from anomalous scattering data collected from crystals derivatized with CH_3Hg^+ to covalently label cysteine residues. The experimentally phased maps were of sufficient quality to model the majority of the structure (fig. S5) and the final TRAAK model was refined to R_{work}/R_{free}= 31.7 / 32.3% with good geometry (table S1).

TRAAK crystallized in space group $p2_12_12_1$ with two protomers, each containing two non-identical pore domains - pore domain 1 and pore domain 2 - in the asymmetric unit forming a single K^+ channel with a molecular two-fold axis (along the K^+ conduction pathway) non-coincident with crystal symmetry axes (fig. S6). Viewed from the bilayer plane, the transmembrane region of the channel spans ~35 Å in height and is formed by the outer helix, pore helix, K^+ selectivity filter, and inner helix from the four pore domains (Fig. 2A). Extensions of the inner helices and the linker between pore domains 1 and 2 protrude ~10 Å

further into the cytoplasmic side. On the extracellular side of the transmembrane region there is a structural unit we term the helical cap extending ~35 Å above the membrane. The helical cap is not observed in other ion channels of known structure. When viewed from the cytoplasmic side of the membrane the channel is rhomboid shaped; the inner helices of pore domain 1 are separated by ~75 Å across a long axis, while the inner helices of pore domain 2 are separated by ~50 Å across a short axis (Fig. 2B).

Structural asymmetry in TRAAK

Structural differences between pore domains 1 and 2 in each protomer of TRAAK result in deviation from the four-fold symmetry of known K^+ channel structures and generate an approximately two-fold symmetric channel instead (Fig. 2C). Differences between TRAAK pore domains 1 and 2 are most evident in three regions: the outer helix to pore helix connection, the filter to inner helix connection, and the inner helix (fig. S7A).

The difference between the outer helix to pore helix connection in pore domains 1 and 2 is shown in fig. S7B. In pore domain 1, the ~60 amino acid long connection forms a two-helix hairpin extending ~35 Å into the extracellular solution. The helices from each protomer pack together to form the helical cap and are covalently linked by a disulfide bond between inter-helix turns at the cap apex. A conserved glycine allows a tight turn at the bottom of the second helix leading to an extended loop containing the N-linked glycosylation sites and connecting to the pore helix. The outer helix to pore helix connection in pore domain 2 forms a short 4 residue linker structurally similar to the corresponding “turret” regions in the prokaryotic K^+ channel MthK (25) and non-selective cation channel NaK (26) (fig. S8).

The difference between the selectivity filter to inner helix connection in pore domains 1 and 2 is shown in fig. S7C. This connection in pore domain 1 is short and forms an interaction network conserved in most K^+ channel structures tethering the extracellular end of the outer helix and inner helix (fig. S9). This connection in pore domain 2 is longer and forms an extended bridge to the inner helix. The interaction network observed in pore domain 1 is not present due to the extended linker and lateral displacement of the pore domain 2 inner helix from the channel core.

The difference between the inner helix in pore domains 1 and 2 is shown in fig. S7D. The pore domain 1 inner helix is kinked halfway through the bilayer and projects towards the cytoplasmic side at an angle ~25° more acute to the membrane plane than the pore domain 2 inner helix. P155, two residues C-terminal to the hinge glycine conserved in all K^+ channels, permits this helix distortion due to its lack of a hydrogen bond donor at the backbone amide position. P155 is conserved in K2P channel pore domain 1 inner helices (except in the THIK-1,2 (fig. S2)) and not observed in pore domain 2 or in other ion channels. The pore domain 1 inner helix is also longer by three helical turns that lead to the cytoplasmic connection between pore domains 1 and 2.

Convergent four-fold symmetry at the selectivity filter

The pore helix and selectivity filter are the most conserved regions of K^+ channels. The majority of K^+ channel selectivity filters share the canonical sequence TxGYGDx (where x denotes a hydrophobic amino acid). In TRAAK, the selectivity filter is made from the sequences TVGYGNY (pore domain 1) and TIGFGDV (pore domain 2). Comparison of TRAAK to the prototypical K^+ channel KcsA (27) demonstrates that the overall two-fold symmetric channel converges to an essentially four-fold symmetric pore helix and selectivity filter (Fig. 3). Only minor deviations due to conservative side chain substitutions between the two TRAAK pore domains are observed. The atomic positions of K^+ coordinating oxygens from selectivity filter residues in TRAAK align well with those from

KcsA (r.m.s.d. 0.6 Å). We model four K^+ ions in positions S1 to S4 and a fifth ion in the extracellular site S0 based on observed electron density from native crystals grown in 150 mM KCl, Tl^+ positions in derivative crystals determined from anomalous scattering data, and chemical knowledge of the ion conduction pathway. The convergence to nearly perfect four-fold symmetry at the pore helix and selectivity filter in the two-fold symmetric TRAAK channel implies strong evolutionary pressures maintaining the integrity of nature's solution to highly selective K^+ conduction through an ion channel.

The TRAAK helical cap structure and implications for K^+ access and pharmacology

The helical cap is unprecedented in ion channel structures and is likely a conserved feature of K2P channels. The interface between protomers is large (~850 $Å^2$) and forms a complementary hydrophobic core (Fig. 4A,B). The region is conserved in length among K2P channels with residues that form the hydrophobic core more conserved than those solvent exposed (fig. S2). The inter-protomer disulfide bonded cysteine is conserved in most K2P channels (fig. S2) and was correctly predicted to covalently link TWIK protomers (28). The TRAAK helical cap is modestly askew of the molecular two-fold axis along the ion conduction pathway. This is presumably the result of crystal packing between the helical cap from one channel and a neighboring channel in the crystal (fig. S6). As a result, residues 55–60 from one protomer are extended while the rest of the cap displays approximate two-fold symmetry.

What might be the functional ramifications of the helical cap? The rigid helical bundle of the cap is positioned above the mouth of the channel pore tethered to pore domain 1 outer helices, bridging opposite sides of the channel. The surface of the helical cap is far enough above the pore entrance to allow unhindered K^+ access from two sides. However, the cap blocks K^+ access from above and from the two tethered sides, creating a bifurcated extracellular pathway for ions to the pore (Fig. 4A,C). Consistently, we observe a Tl^+ ion along one branch of the split pathway to the pore in crystals grown in the presence of $TlNO_3$ in place of KCl (Fig. 4A,C).

K2P channels are not responsive to known K^+ channel blockers including pore-blocking toxins from the extracellular side (6, 16). The TRAAK structure provides a simple explanation for these observations: the presence of the helical cap above the pore would sterically prevent toxin access to the channel mouth. A similar steric occlusion mechanism was proposed for Kir2.2 based on its atypically tall turrets surrounding the pore entrance (29). By fully preventing access to the mouth of the channel from above and two sides, the helical cap in K2P channels more dramatically restricts molecular access to the pore entryway.

Implications of TRAAK structure for channel gating

The crystal structure of TRAAK has an open inner helical gate (Fig. 2C). The central cavity under the selectivity filter is wide and forms a vestibule continuous with the cytoplasmic solution presenting no steric hindrance to ion flux. The pore domain 1 inner helices are wide open with the smallest constriction measuring ~12 Å, similar to the most open configuration observed in MthK (fig. S10) (25). The pore domain 2 inner helices are slightly less open, with the smallest constriction measuring ~10 Å, but this is still more open than observed in open-state Kv structures (fig. S10) (30).

It is interesting to speculate on the potential for inner helix gating in TRAAK. Recent studies have suggested that the closely related K2P TREK-1 has an inner gate that is

constitutively open (31, 32). Three features of the TRAAK pore domain 1 inner helix may be relevant if TRAAK has a similarly constitutively open inner gate: the presence of P155 that kinks the helix, the nature of the putative membrane interaction region (discussed below), and the peptide linkage to the pore domain 2 outer helix. The combination of these structural features may restrict the ability of the pore domain 1 inner helix to access a closed inner gate conformation.

TRAAK (and TREK) channels are exquisitely responsive to the chemical and mechanical properties of the lipid bilayer. Chemically, TRAAK is activated by arachidonic acid, other polyunsaturated fatty acids, and lysophosphatidic acidby an apparently direct mechanism (16, 33–35). Mechanically, applying the equivalent to positive (and not negative) intracellular pressure through a patch pipette reversibly activates TRAAK and TREK (21, 34), while hyperosmolarity-induced cell shrinkage reduces TREK currents (20). Pressure-induced activation of TRAAK is enhanced upon cytoskeletal disruption or patch excision suggesting that TRAAK directly responds to the physical state of the bilayer (21).

What might be the molecular sensor(s) of the mechanical and chemical state of the bilayer in TRAAK? In TREK channels, a region immediately C-terminal to the intracellular end of the pore domain 2 inner helix has been demonstrated to be involved in activity modulation by mechanical force, lipids and fatty acids, acidic pH_i, phosphorylation, and interaction with the accessory protein AKAP150 (20, 36–40). The homologous C-terminal region in TRAAK is included in the crystal construct and is partially modeled as a cytoplasmic extension of the pore domain 2 inner helix (Fig. 2). However, this region has not been shown to be involved in TRAAK modulation: TRAAK is not activated by acidic pH_i, TRAAK does not interact with AKAP150, and chimeras exchanging this region with that from TASK K2P channels display unaltered response to arachidonic acid and mechanical force (34, 36, 39, 41). Together these data suggest that an alternative molecular sensor is utilized for TRAAK lipid- and mechano-activation.

A distinctive structural feature of TRAAK is illustrated in Fig. 5A. After the kink at P155, the pore domain 1 inner helix projects laterally and runs approximately parallel to the cytoplasmic membrane surface. Along this projection the helix is amphipathic. Hydrophobic residues point towards the lipid bilayer along one face opposite a series of basic residues (R167, R173, H174, H178) pointed towards the membrane/cytoplasm interface. An additional basic residue (K185) further along the helix is also directed towards the same plane. These five residues are conserved in basic character among TRAAK channels (fig. S3). The amphipathic helix is thus positioned to interact with both the hydrophobic tails and acidic headgroups of membrane lipids. This structured extension of the pore domain 1 inner helix, which extends like a tendril out into the lipid membrane inner leaflet, may be related to this channel's ability to respond to both mechanical and chemical properties of the cell membrane.

Another consequence of the inner helix structure in TRAAK is illustrated in Fig. 5B. The relative orientation of inner helices creates an extended lateral opening to the central cavity from the membrane. Between the two protomers, a gap ~5 Å wide extends through the bilayer from the bottom of the selectivity filter to the ends of the pore domain 2 inner helix and pore domain 1 outer helix on the cytoplasmic side. While we observe electron density from the central cavity to the lateral openings in TRAAK, we are not able to confidently assign and model a ligand at this resolution. Lateral openings have been observed in other ion channels, including the K^+ channel KcsA (27) and the voltage-gated sodium channel (42), but the size and shape of the openings in TRAAK are striking. This bilayer-facing opening results in a large protein surface accessible to the membrane and is a potential site for the interaction of lipids and other hydrophobic molecules with the TRAAK channel.

Supplementary Material

Refer to Web version on PubMed Central for supplementary material.

Acknowledgments

We thank Michael Becker, Ruslan Sanishvili, and staff at beamline 23-IDB/D at the APS, Frank Murphy, Kanagalaghatta Rajashankar, and staff at beamline 24-IDC at the APS, and Howard Robinson and staff at beamline X29 at NSLS for assistance at the synchrotrons, and members of the MacKinnon laboratory for helpful discussions. S.G.B. is a postdoctoral fellow of the Helen Hay Whitney Foundation, Josefina del Mármol is a Howard Hughes Medical Institute International Student Research Fellow, and R.M. is an investigator in the Howard Hughes Medical Institute. The authors declare no conflict of interest.

The x-ray crystallographic coordinates and structure factors will be released under the entry 3UM7 in the Protein Data Bank upon publication of the manuscript.

S.G.B designed, purified, and crystallized TRAAK, collected, processed and refined crystallographic data, and performed the flux assay, and analyzed data. J.M. performed and analyzed data from electrophysiology experiments in CHO cells. R.M. performed and analyzed data from bilayer experiments. S.G.B and R.M. wrote the paper.

References

1. Hille, B. Ion channels of excitable membranes. Sinauer Associates Inc; Sunderland, MA: 2001.
2. Hodgkin AL, Huxley AF. Potassium leakage from an active nerve fibre. J Physiol. 1947; 106:341. [PubMed: 16991765]
3. Enyedi P, Czirjak G. Molecular background of leak K+ currents: two-pore domain potassium channels. Physiol Rev. 90:559. [PubMed: 20393194]
4. Ketchum KA, Joiner WJ, Sellers AJ, Kaczmarek LK, Goldstein SA. A new family of outwardly rectifying potassium channel proteins with two pore domains in tandem. Nature. 1995; 376:690. [PubMed: 7651518]
5. Zhou XL, Vaillant B, Loukin SH, Kung C, Saimi Y. YKC1 encodes the depolarization-activated K+ channel in the plasma membrane of yeast. FEBS Lett. 1995; 373:170. [PubMed: 7589459]
6. Lesage F, et al. TWIK-1, a ubiquitous human weakly inward rectifying K+ channel with a novel structure. EMBO J. 1996; 15:1004. [PubMed: 8605869]
7. Cohen A, Ben-Abu Y, Zilberberg N. Gating the pore of potassium leak channels. Eur Biophys J. 2009; 39:61. [PubMed: 19404634]
8. Mathie A, Al-Moubarak E, Veale EL. Gating of two pore domain potassium channels. J Physiol. 588:3149. [PubMed: 20566661]
9. Patel AJ, et al. Inhalational anesthetics activate two-pore-domain background K+ channels. Nat Neurosci. 1999; 2:422. [PubMed: 10321245]
10. Cotten JF, Keshavaprasad B, Laster MJ, Eger EI 2nd, Yost CS. The ventilatory stimulant doxapram inhibits TASK tandem pore (K2P) potassium channel function but does not affect minimum alveolar anesthetic concentration. Anesth Analg. 2006; 102:779. [PubMed: 16492828]
11. Duprat F, et al. The neuroprotective agent riluzole activates the two P domain K(+) channels TREK-1 and TRAAK. Mol Pharmacol. 2000; 57:906. [PubMed: 10779373]
12. Heurteaux C, et al. Deletion of the background potassium channel TREK-1 results in a depression-resistant phenotype. Nat Neurosci. 2006; 9:1134. [PubMed: 16906152]
13. Lafreniere RG, et al. A dominant-negative mutation in the TRESK potassium channel is linked to familial migraine with aura. Nat Med. 16:1157. [PubMed: 20871611]
14. Barel O, et al. Maternally inherited Birk Barel mental retardation dysmorphism syndrome caused by a mutation in the genomically imprinted potassium channel KCNK9. Am J Hum Genet. 2008; 83:193. [PubMed: 18678320]
15. Bang H, Kim Y, Kim D. TREK-2, a new member of the mechanosensitive tandem-pore K+ channel family. J Biol Chem. 2000; 275:17412. [PubMed: 10747911]
16. Fink M, et al. A neuronal two P domain K+ channel stimulated by arachidonic acid and polyunsaturated fatty acids. EMBO J. 1998; 17:3297. [PubMed: 9628867]

17. Fink M, et al. Cloning, functional expression and brain localization of a novel unconventional outward rectifier K+ channel. EMBO J. 1996; 15:6854. [PubMed: 9003761]
18. Kang D, Choe C, Kim D. Thermosensitivity of the two-pore domain K+ channels TREK-2 and TRAAK. J Physiol. 2005; 564:103. [PubMed: 15677687]
19. Maingret F, et al. TREK-1 is a heat-activated background K(+) channel. EMBO J. 2000; 19:2483. [PubMed: 10835347]
20. Patel AJ, et al. A mammalian two pore domain mechano-gated S-like K+ channel. EMBO J. 1998; 17:4283. [PubMed: 9687497]
21. Maingret F, Fosset M, Lesage F, Lazdunski M, Honore E. TRAAK is a mammalian neuronal mechano-gated K+ channel. J Biol Chem. 1999; 274:1381. [PubMed: 9880510]
22. Noel J, et al. The mechano-activated K+ channels TRAAK and TREK-1 control both warm and cold perception. EMBO J. 2009; 28:1308. [PubMed: 19279663]
23. Opsahl LR, Webb WW. Lipid-glass adhesion in giga-sealed patch-clamped membranes. Biophys J. 1994; 66:75. [PubMed: 8130347]
24. Lesage F, Maingret F, Lazdunski M. Cloning and expression of human TRAAK, a polyunsaturated fatty acids-activated and mechano-sensitive K(+) channel. FEBS Lett. 2000; 471:137. [PubMed: 10767409]
25. Ye S, Li Y, Jiang Y. Novel insights into K+ selectivity from high-resolution structures of an open K+ channel pore. Nat Struct Mol Biol. 17:1019. [PubMed: 20676101]
26. Alam A, Jiang Y. High-resolution structure of the open NaK channel. Nat Struct Mol Biol. 2009; 16:30. [PubMed: 19098917]
27. Zhou Y, Morais-Cabral JH, Kaufman A, MacKinnon R. Chemistry of ion coordination and hydration revealed by a K+ channel-Fab complex at 2.0 A resolution. Nature. 2001; 414:43. [PubMed: 11689936]
28. Lesage F, et al. Dimerization of TWIK-1 K+ channel subunits via a disulfide bridge. EMBO J. 1996; 15:6400. [PubMed: 8978667]
29. Tao X, Avalos JL, Chen J, MacKinnon R. Crystal structure of the eukaryotic strong inward-rectifier K+ channel Kir2.2 at 3.1 A resolution. Science. 2009; 326:1668. [PubMed: 20019282]
30. Long SB, Tao X, Campbell EB, MacKinnon R. Atomic structure of a voltage-dependent K+ channel in a lipid membrane-like environment. Nature. 2007; 450:376. [PubMed: 18004376]
31. Bagriantsev SN, Peyronnet R, Clark KA, Honore E, Minor DL Jr. Multiple modalities converge on a common gate to control K(2P) channel function. EMBO J. 30:3594. [PubMed: 21765396]
32. Piechotta PL, et al. The pore structure and gating mechanism of K2P channels. EMBO J. 30:3607. [PubMed: 21822218]
33. Maingret F, Patel AJ, Lesage F, Lazdunski M, Honore E. Lysophospholipids open the two-pore domain mechano-gated K(+) channels TREK-1 and TRAAK. J Biol Chem. 2000; 275:10128. [PubMed: 10744694]
34. Kim Y, Bang H, Gnatenco C, Kim D. Synergistic interaction and the role of C-terminus in the activation of TRAAK K+ channels by pressure, free fatty acids and alkali. Pflugers Arch. 2001; 442:64. [PubMed: 11374070]
35. Chemin J, et al. Lysophosphatidic acid-operated K+ channels. J Biol Chem. 2005; 280:4415. [PubMed: 15572365]
36. Sandoz G, et al. AKAP150, a switch to convert mechano-, pH- and arachidonic acid-sensitive TREK K(+) channels into open leak channels. EMBO J. 2006; 25:5864. [PubMed: 17110924]
37. Murbartian J, Lei Q, Sando JJ, Bayliss DA. Sequential phosphorylation mediates receptor- and kinase-induced inhibition of TREK-1 background potassium channels. J Biol Chem. 2005; 280:30175. [PubMed: 16006563]
38. Chemin J, et al. A phospholipid sensor controls mechanogating of the K+ channel TREK-1. EMBO J. 2005; 24:44. [PubMed: 15577940]
39. Honore E, Maingret F, Lazdunski M, Patel AJ. An intracellular proton sensor commands lipid- and mechano-gating of the K(+) channel TREK-1. EMBO J. 2002; 21:2968. [PubMed: 12065410]

40. Kim Y, Gnatenco C, Bang H, Kim D. Localization of TREK-2 K+ channel domains that regulate channel kinetics and sensitivity to pressure, fatty acids and pHi. Pflugers Arch. 2001; 442:952. [PubMed: 11680629]
41. Maingret F, Patel AJ, Lesage F, Lazdunski M, Honore E. Mechano- or acid stimulation, two interactive modes of activation of the TREK-1 potassium channel. J Biol Chem. 1999; 274:26691. [PubMed: 10480871]
42. Payandeh J, Scheuer T, Zheng N, Catterall WA. The crystal structure of a voltage-gated sodium channel. Nature. 475:353. [PubMed: 21743477]
43. Kawate T, Gouaux E. Fluorescence-detection size-exclusion chromatography for precrystallization screening of integral membrane proteins. Structure. 2006; 14:673. [PubMed: 16615909]
44. Minor W, Cymborowski M, Otwinowski Z, Chruszcz M. HKL-3000: the integration of data reduction and structure solution--from diffraction images to an initial model in minutes. Acta Crystallogr D Biol Crystallogr. 2006; 62:859. [PubMed: 16855301]
45. Strong M, et al. Toward the structural genomics of complexes: crystal structure of a PE/PPE protein complex from Mycobacterium tuberculosis. Proc Natl Acad Sci U S A. 2006; 103:8060. [PubMed: 16690741]
46. McCoy AJ, et al. Phaser crystallographic software. J Appl Crystallogr. 2007; 40:658. [PubMed: 19461840]
47. Sheldrick GM. A short history of SHELX. Acta Crystallogr A. 2008; 64:112. [PubMed: 18156677]
48. Vonrhein C, Blanc E, Roversi P, Bricogne G. Automated structure solution with autoSHARP. Methods Mol Biol. 2007; 364:215. [PubMed: 17172768]
49. Read RJ, McCoy AJ. Using SAD data in Phaser. Acta Crystallogr D Biol Crystallogr. 67:338. [PubMed: 21460452]
50. Emsley P, Lohkamp B, Scott WG, Cowtan K. Features and development of Coot. Acta Crystallogr D Biol Crystallogr. 66:486. [PubMed: 20383002]
51. Murshudov GN, et al. REFMAC5 for the refinement of macromolecular crystal structures. Acta Crystallogr D Biol Crystallogr. 67:355. [PubMed: 21460454]
52. Schroder GF, Levitt M, Brunger AT. Super-resolution biomolecular crystallography with low-resolution data. Nature. 464:1218. [PubMed: 20376006]
53. Schmidt D, Cross SR, MacKinnon R. A gating model for the archeal voltage-dependent K(+) channel KvAP in DPhPC and POPE:POPG decane lipid bilayers. J Mol Biol. 2009; 390:902. [PubMed: 19481093]
54. Winn MD, et al. Overview of the CCP4 suite and current developments. Acta Crystallogr D Biol Crystallogr. 67:235. [PubMed: 21460441]
55. Schrodinger LLC. 2010
56. Katoh K, Kuma K, Toh H, Miyata T. MAFFT version 5: improvement in accuracy of multiple sequence alignment. Nucleic Acids Res. 2005; 33:511. [PubMed: 15661851]
57. Waterhouse AM, Procter JB, Martin DM, Clamp M, Barton GJ. Jalview Version 2--a multiple sequence alignment editor and analysis workbench. Bioinformatics. 2009; 25:1189. [PubMed: 19151095]
58. Yu FH, Yarov-Yarovoy V, Gutman GA, Catterall WA. Overview of molecular relationships in the voltage-gated ion channel superfamily. Pharmacol Rev. 2005; 57:387. [PubMed: 16382097]

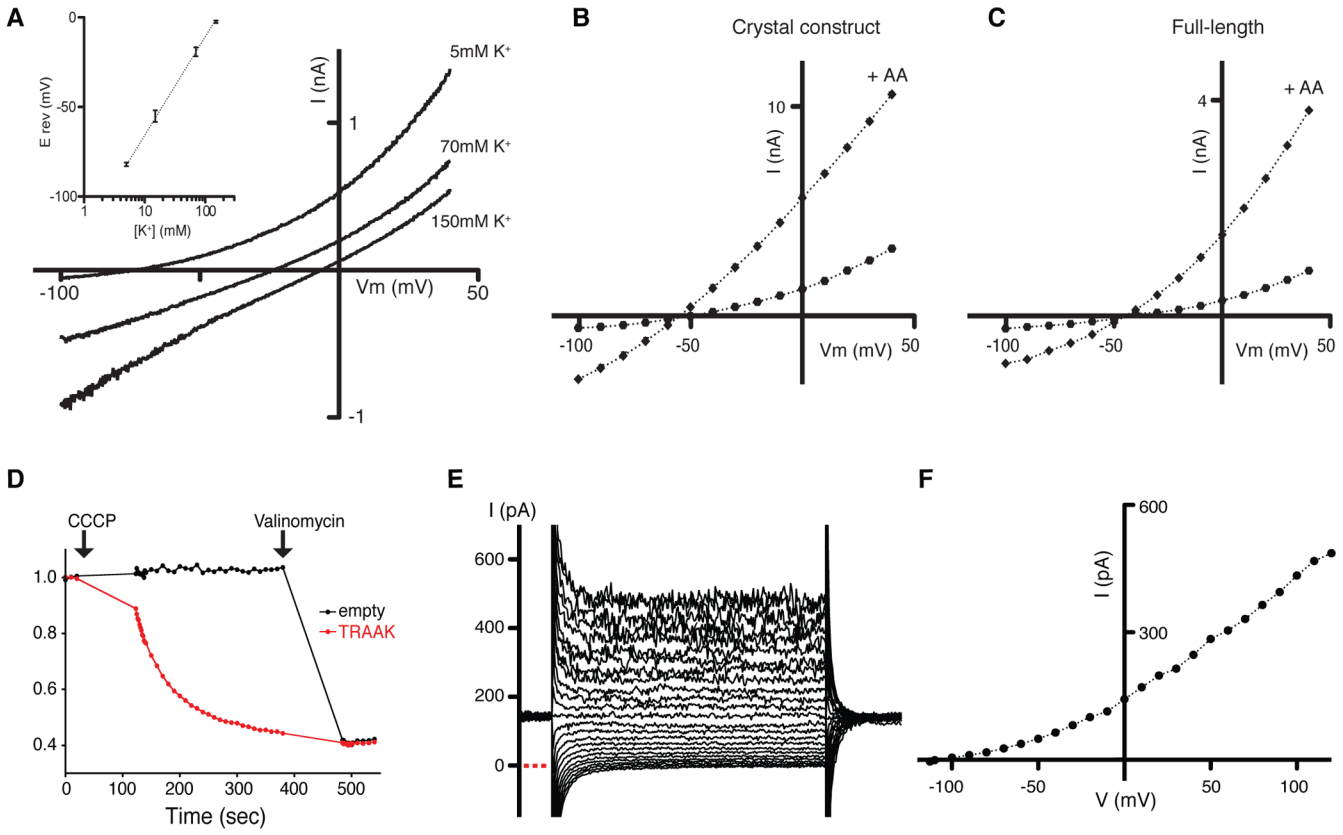

Fig. 1. Analysis of TRAAK channel activity

(A) Macroscopic currents from CHO cells expressing the crystal construct of TRAAK. **(A)** Current-voltage relationship during voltage ramp. Current was measured in whole cell mode during a voltage ramp from −100 mV to 40 mV from a holding potential of −80 mV in 800 msec. Curves recorded from cells in 5, 70, and 150 mM external [K^+] are displayed. Reversal potential determined from voltage ramps recorded from cells in 5, 15, 70, and 150 mM external [K^+] is plotted in the inset. **(B)** Arachidonic acid (AA) activation of the crystal construct of the TRAAK channel. **(C)** Arachidonic acid (AA) activation of the full-length channel. Current-voltage relationship is plotted from whole-cell recordings during voltage pulses from −100 to 40 mV from a holding potential of −80 mV before and after perfusion of arachidonic acid (+AA). **(D)** K^+ flux assay in which K^+ efflux drives the carbonyl cyanide *m*-chlorophenyl hydrazone (CCCP)-mediated uptake of protons, which are detected by fluorophore 9-amino-6-chloro-2-methoxyacridine (ACMA). Vesicles were loaded with 150 mM K^+, 0 mM Na^+ and assayed in buffer with 0 mM K^+, 150 mM Na^+. Relative fluorescence change recorded from TRAAK reconstituted (red) and empty (black) lipid vesicles is shown. Addition of the K^+ ionophore valinomycin results in flux from crystal construct TRAAK reconstituted and empty vesicles. **(E)** Current recorded from TRAAK reconstituted into planar lipid bilayers under bi-ionic conditions. Current was recorded during voltage pulses from −120 mV to 120 mV from a holding potential of 0 mV with internal 150 mM K^+, 0 mM Na^+ and external 0 mM K^+, 150 mM Na^+ by electrophysiological convention. Zero current level is indicated with a dotted red line. **(F)** Current-voltage relationship plotted from data in **(E)**.

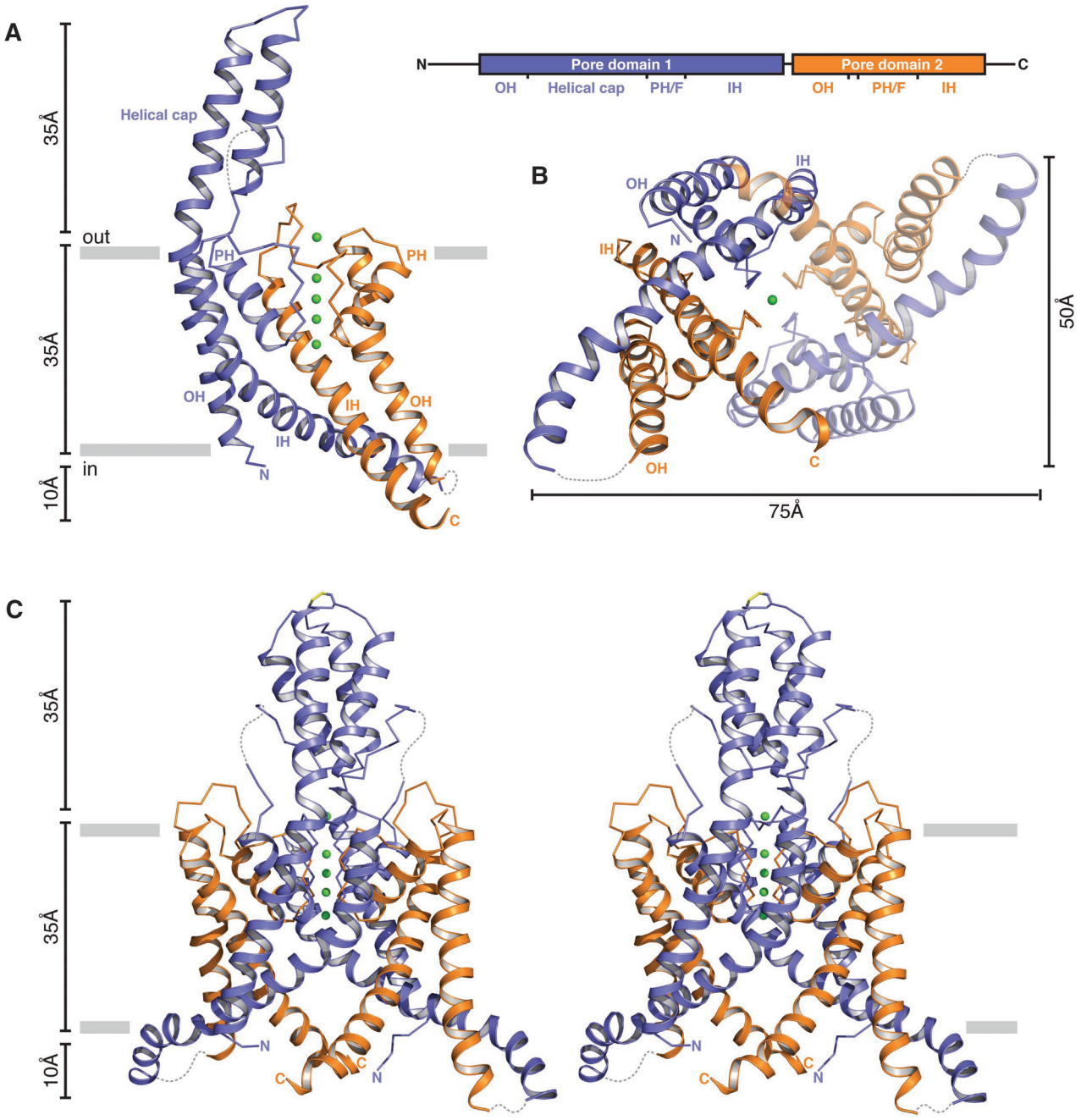

Fig. 2. Structure of TRAAK

(A) Ribbon representation of a single TRAAK protomer viewed from the membrane plane with the extracellular solution above (left). Approximate positions of the lipid bilayer boundaries are indicated as gray bars. Pore domain 1 is colored blue, pore domain 2 is colored orange, and potassium ions are shown as green spheres. Illustration of TRAAK protomer organization (right). Approximate boundaries of structural features are indicated in the illustration and labeled in the structure (N and C terminus, outer helix (OH), helical cap, pore helix (PH), selectivity filter (F), and inner helix (IH)). **(B)** A view of the TRAAK channel from the cytoplasmic solution. The protomer shown in **(A)** is rotated 90 both into the page and clockwise and the second protomer is half transparent. **(C)** Stereo view of

TRAAK viewed from the membrane plane with the protomer shown in **(A)** rotated 90 . The disulfide bond bridging the apex of the helical cap is shown in stick representation with the cysteine sulfur colored yellow. Note that part of the cytoplasmic extension of protomer B (residues 180–187) is not present in the final TRAAK model due to weak electron density features. Here it is modeled from a superposition of the well-defined region in protomer A for visual clarity. Loops not modeled in the structure due to lack of interpretable electron density are drawn as dashed gray lines.

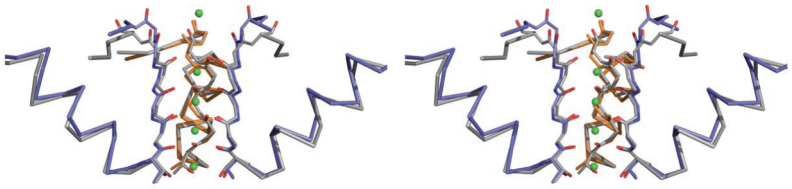

Fig. 3. Convergent symmetry of the TRAAK pore helices and selectivity filter

Stereo view, from the membrane plane with extracellular solution above, shows a comparison between the TRAAK and KcsA (27) pore helices and selectivity filters. Pore helices and selectivity filter chains closest to the viewer are removed. Pore helices are shown as wires and selectivity filters as backbone sticks. TRAAK pore domain 1 is blue, TRAAK pore domain 2 is orange, and KcsA is gray with backbone carbonyl and threonine hydroxyl oxygen atoms from selectivity filter residues shown in red. K^+ positions in TRAAK (green spheres) occupy canonical positions S0–S4 from the extracellular to intracellular side.

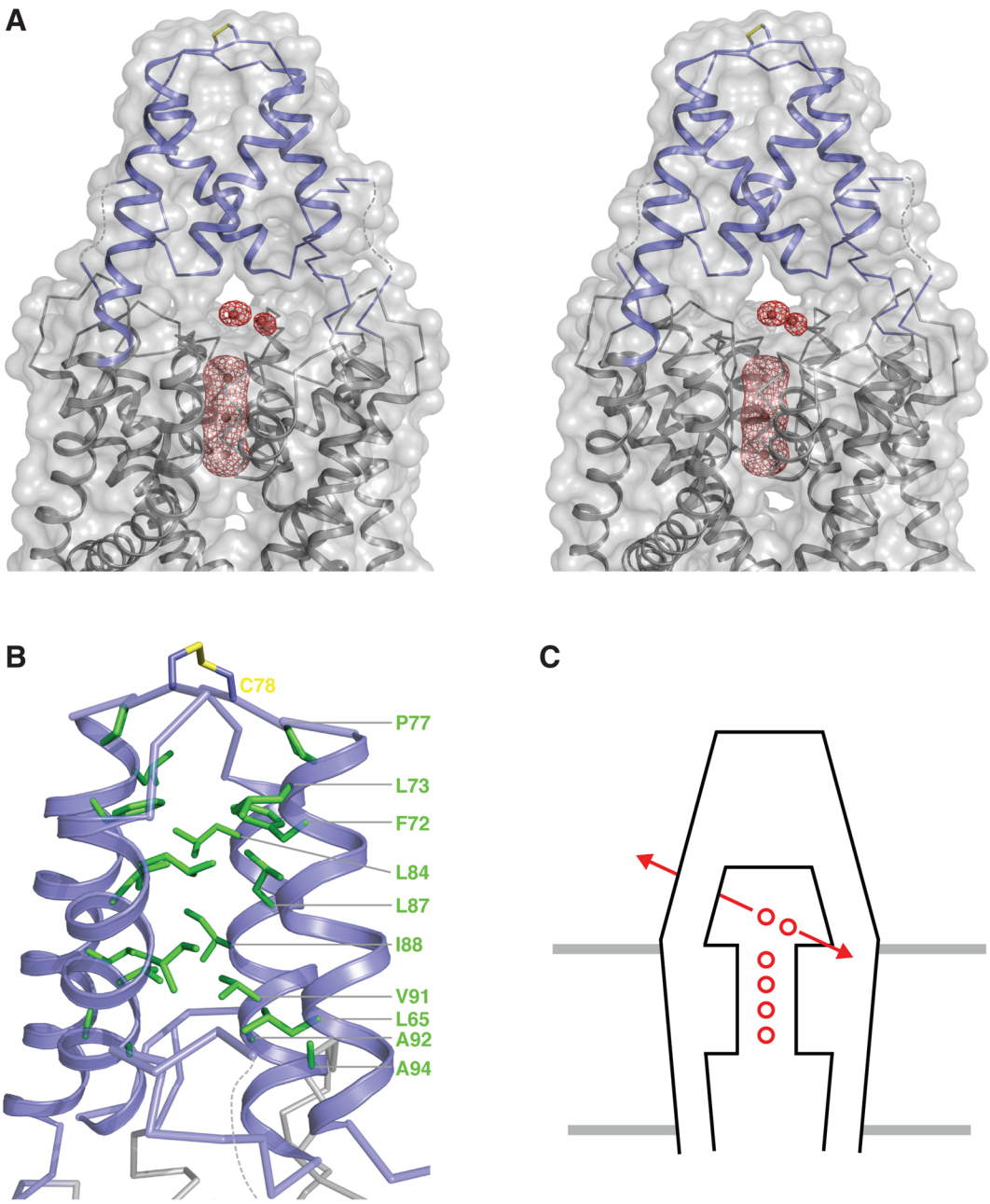

Fig. 4. The TRAAK helical cap

(A) Stereo view of the helical cap viewed from the membrane plane with the extracellular solution above. TRAAK is shown as grey ribbons with the helical cap blue within a semi-transparent surface representation. A Tl^+ anomalous-difference Fourier map (red mesh) calculated from 30–4.2 Å and contoured at 6σ is shown around Tl^+ ions (red spheres). **(B)** The hydrophobic core of the helical cap. The helical cap is shown as a blue ribbon with hydrophobic residues (L65, F72, L73, P77, L84, L87, I88, V91, A92, A94) as green sticks. The C78 disulfide bond is shown as blue sticks with yellow sulfur atoms. **(C)** Cartoon depiction of the bifurcated ion pathway created by the TRAAK helical cap. View is analogous to **(A)**. TRAAK (black) in a membrane (gray) coordinates four ions (red circles) in the selectivity filter and one ion directly above in site S0. A sixth ion is present in one of

the two possible extracellular access/egress pathways (red arrows) that extend into the page and towards the viewer. The TRAAK helical cap blocks ion access from above and laterally in the image plane.

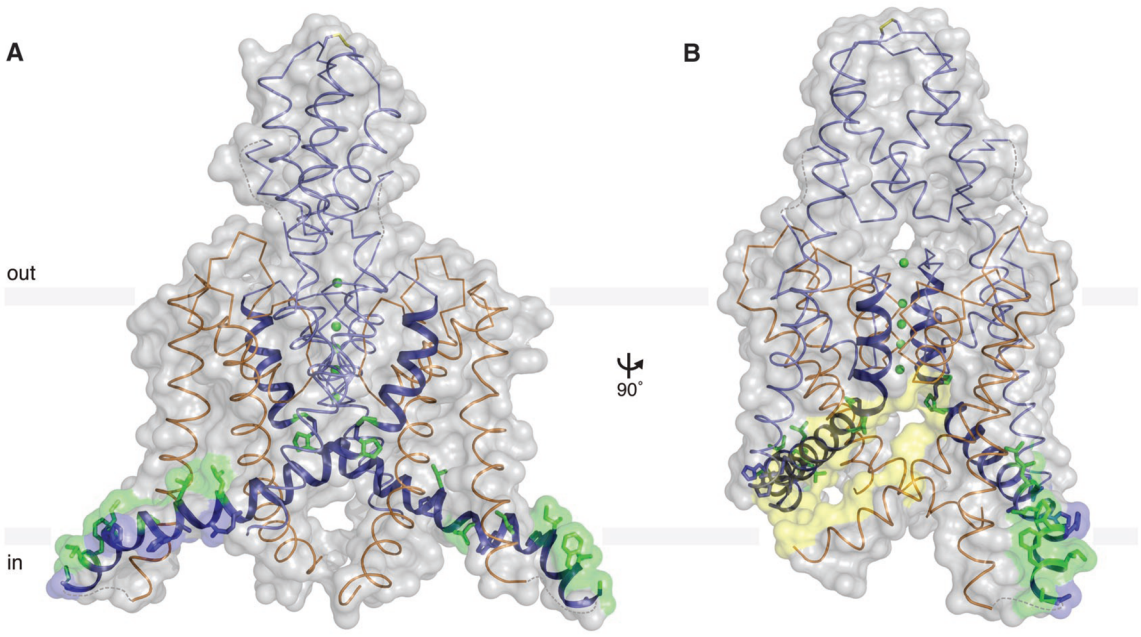

Fig. 5. TRAAK channel inner helices and gating implications

(A) View from the membrane with extracellular solution above of the amphipathic segment of the pore domain 1 inner helix (as in Fig. 1C). TRAAK is shown in wire representation with inner helices from pore domain 1 as ribbons and key residues as sticks within a semi-transparent gray surface. Pore domain 1 is colored blue, pore domain 2 is colored orange, and K^+ ions are shown as green spheres. The hinge glycine (G153), kink proline (P155), and hydrophobic face of the amphipathic segment (L168, L172, I176, I179, I182, F183, W186) are colored green. Basic residues conserved in TRAAK (R167, R173, H174, H178, K185) on the solution accessible face of the amphipathic helix are colored blue. **(B)** A view rotated 90 with respect to **(A)**. The lipid bilayer accessible surface of the lateral opening into the TRAAK channel central cavity closest to the viewer is additionally colored yellow.